

Medicinal Electrochemistry of Halogenated and Nitrated Pterocarpanquinones

Thaissa L. Silva,^{a,b} Julio C. S. da Silva,^a Dimas J. P. Lima,^a Fabricia R. Ferreira,^a
Camila C. de Vasconcelos,^{a,c} Danyelle C. Santos,^b Chaquip D. Netto,^{d,e} Paulo R. R. Costa^d
and Marília O. F. Goulart^{ib*,a}

^aInstituto de Química e Biotecnologia, Universidade Federal de Alagoas, 57072-970 Maceió-AL, Brazil

^bNúcleo de Ciências Exatas (NCEX), Universidade Federal de Alagoas, Campus de Arapiraca,
57309-005 Arapiraca-AL, Brazil

^cCentro Universitário CESMAC, R. da Harmonia, 57081-350 Maceió-AL, Brazil

^dLaboratório de Química Bioorgânica, Núcleo de Pesquisas de Produtos Naturais,
Centro de Ciências da Saúde, Bloco H, Universidade Federal do Rio de Janeiro,
21941-590 Rio de Janeiro-RJ, Brazil

^eLaboratório de Química, Universidade Federal do Rio de Janeiro,
Campus Professor Aloísio Teixeira, 27930-560 Macaé-RJ, Brazil

Electrochemical methods are considered useful tools for simulations of biological redox reactions. The activities of quinones depend on their bioreduction. Biologically active pterocarpanquinones **LQB-149** (nitroderivative), **150** and **151** (bromo and chloroderivatives, respectively) were electrochemically investigated by cyclic voltammetry, differential pulse voltammetry, and *in situ* UV-Vis spectroelectrochemistry, in aprotic media (*N,N*-dimethylformamide (DMF) + tetra-*N*-butylammonium (TBAPF₆)). The data obtained regarding their reduction mechanisms, positive reactivity with oxygen and analysis of the electrogenerated intermediates were useful in explaining their biological outcomes. The appearance of bands at 397 and 480 nm, for the halogenated compounds, suggests the generation of transient quinonemethides (QM), electrophilic intermediates related to their activity. As an additional proof for the intermediacy of QM, in the redox processes, chemical reduction of **LQB-150**, in the presence of hexanethiol was performed and led to a thioalkylated quinone. For the nitroderivative, a broad band appeared at 432 nm, corresponding to the generation of the nitroradical anion, giving rise to a dianion diradical, after reduction at the second wave potential. Computational data correlate well with electrochemical experiments. Homogeneous electron transfer to oxygen, yielding reactive oxygen species, the generation of electrophilic species and the radical reactivity, explain partially the mechanism of biological action.

Keywords: pterocarpanquinones, electrochemical parameters, multi-redox systems, UV-Vis spectroelectrochemistry, bioreduction

Introduction

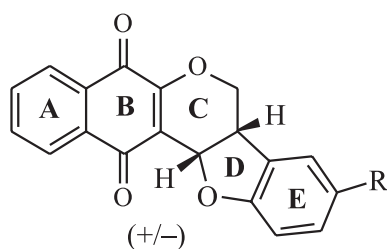
Quinones are double-edged sword compounds. They can create a variety of hazardous effects *in vivo* including acute cytotoxicity, immunotoxicity, and carcinogenesis, and, in contrast, can induce cytoprotection and be relevant medicines against several diseases.¹ The molecular pathways related to this bioactivity/toxicity of quinones include oxidative stress (OS) enhancement, bioreductive alkylation through the

generation of electrophilic intermediates with consequent Michael addition of various nucleophilic endobiotics, and also through metal complexation, with similar mechanisms and sometimes increased effects.^{1,2} On this line, modulation of redox signaling, through specific interaction with enzymes, nuclear factors and receptors, is also, an important pathway.³ Quinones can also work as DNA intercalators, inhibitors of topoisomerases and of some enzymes of the mitochondrial electron transfer chain.^{2,3}

Several pterocarpanquinones, hybrid quinones prepared from pterocarpan (flavonoids) and lapachol had been

*e-mail: mariliaof@gmail.com

synthesized and successfully screened in terms of biological and pharmacological activities. Some of the most active were **LQBs-118, 149, 150** and **151** (Figure 1).⁴



LQB-118 - R = H

LQB-149 - R = NO₂

LQB-150 - R = Br

LQB-151 - R = Cl

Figure 1. Structures of pterocarpanquinones.

LQB-118 is a potent anticancer pterocarpanquinone, and its biological activities and mechanisms of action have been extensively reported.^{4,5} This pterocarpanquinone is a developing and orally active pterocarpanquinone agent that effectively induces the programmed cell death of prostate cancer cells, through quinone reduction and reactive oxygen species (ROS) generation. The inhibition of superoxide dismutase 1 (SOD1) expression enhances **LQB-118** activity, presumably by impairing the cellular antioxidant response.^{6,7} This molecule also presents antiparasitic profile.^{5,8}

Since reductive bioactivation could be involved in the molecular mechanism of action of these compounds,^{1,9} the introduction of electron withdrawing groups at the E-ring was worthy investigating, once it could stabilize the phenoxide leaving group, proposed as an intermediate product from chemical and electrochemical reduction.⁵

LQB-149, the nitro derivative of **LQB-118**, was reported to be active against human leukemic cell lines with half maximal inhibitory concentration (IC₅₀) against K562 of 3.48 μM and of 0.40 μM against HL-60,⁷ despite being less selective and more toxic than **LQB-118**, toward normal cells (PBMC), with IC₅₀ of 8.6 μM. It was also assayed against HCT-8 (8.30 μM), SF-295 (8.90 μM) and MDA-MB435 (17.40 μM), being highly selective toward HL-60. **LQB-150** and **LQB-151** present lower cytotoxicity: IC₅₀ against K562 (5.70 and 6.77 μM, respectively) and HL-60 (4.87 μM for both).⁷

LQB-151 is a promising compound for chemotherapy to treat toxoplasmosis. It inhibited *Toxoplasma gondii* growth in LLCMK2 cells with IC₅₀ value lower than 1 μM.⁸ **LQB-149** was also evaluated on *Leishmania amazonensis* in culture: promastigotes and amastigotes (the form

present in the human disease), with IC₅₀ 1.07 and 1.85 μM, respectively. The selectivity index (SI) was calculated for amastigote form using M J7744 cells (murine macrophages) (SI = 6.5) as reference.¹⁰

Physicochemical descriptors for **LQBs-150** and **151** were also reported, suggesting that they adhere to Lipinski's rule.⁸

Progressive overlap of interests between electrochemistry and other areas of research, mainly biologically-based ones, allows the mastering of electrochemical methods and methodologies and approaches scientists from these different areas.² Electrochemical methods are useful tools for simulations of biological (i.e., metabolic) redox reactions. Metabolically active sites, i.e., positions at which the drug is prone to suffer oxidation or reduction, can be rapidly elucidated through electrochemical/computational investigations and possible metabolites can be directly identified.^{2,9} The majority of these intermediates are formed after oxidation of the parent compound or reduction followed by elimination, to generate electrophilic intermediates, which subsequently can react with nucleophilic groups in cellular biomacromolecules, such as lipids, proteins and DNA.²⁻⁴

LQB-118 was recently investigated by electrochemical methods, in protic and aprotic media, towards oxygen, and DNA. UV-Vis spectroelectrochemistry allowed to prove the reduction-based quinonemethide generation and along with DNA positive interaction studies, did well to predict the oxidative stress-based biological activity of the compound.⁵

We, herein, investigated the electrochemical behavior of biologically active halogenated and nitrated pterocarpanquinones, in aprotic media, in the absence and presence of oxygen in order to obtain data regarding their reduction mechanisms, the analysis of the stability of the electrogenerated intermediates, as well as, in the presence of thiols.

The study of compounds carrying multiple redox centers, as part of the molecular system and doubly responsible for specific properties, like in nitroquinones, deserves special attention.¹¹

The presence of an electron-withdrawing group confers stronger oxidant properties on the quinone, but the corresponding hydroquinone or catechol is less readily oxidized. Nitroquinones have been investigated with special toxicological concern. Quinones¹ and nitroaromatics¹¹ are key pharmacophores, activated by electron transfer, coupled with prior or following chemical reactions.

Electroreduction of nitro derivatives of quinones has been described, but, in the majority of cases, without considering any relationship with pharmacological activities and any evidence of mechanistic complications.¹²

The presence of halogens in **LQB-150** and **151** can also contribute to a diverse redox behavior. The electrochemistry of halogenated compounds, mainly aromatic ones (ArX), has been thoroughly investigated on several electrodes.¹³ For halides, bi-electronic uptake in aprotic solvents causes rupture of the C–X bond, by either a concerted or stepwise mechanism, followed by reduction of the ensuing radical to an anion. The latter is usually protonated by residual water to the respective C–H bond.¹³

As the electrophilic character of quinones has been proved to be relevant for several biological activities,² and considering that the presence of a nitro substituent certainly makes the electron capture by the quinone moiety easier,¹² this paper intends to consider the mutual influence of the redox groups on the electron transfer processes of the present pterocarpanquinones (Figure 1) and the structural properties of their electrochemically generated radical anions. The presence of halogens also contribute to the activity and to the electrochemical profile.¹³

In general, naturally important quinones, for instance ubiquinones, and their intermediates semi-ubiquinones, as well as reduced forms exist inside hydrophobic cell membranes.¹⁴ It is advantageous to study their electrochemical properties in trace water environment, such as aprotic organic solvents, which mimic the nonpolar environment in a living cell where the electrochemical properties differ from that observed in aqueous systems.^{2,3,14}

Experimental

Reagents and equipments

Extra-dry *N,N*-dimethylformamide (DMF; 99.8%) was acquired from Acros Organics, tetra-*N*-butylammonium (TBAPF₆) and tetra-*N*-butylammonium perchlorate (TBAP) and the other chemicals from Sigma-Aldrich (St. Louis, USA). TBAPF₆ was purified by recrystallization from absolute ethanol (×3), and dried at

reduced pressure, at 60 °C. All the reagents were analytical grade.

Structural elucidation was performed by using 1D and 2D nuclear magnetic resonance (NMR) spectra, recorded by using a Bruker Avance 400 spectrometer (¹H: 600 and ¹³C: 150 MHz in CDCl₃). Cyclic voltammetry (CV) or differential pulse voltammetry (DPV) experiments were performed with a conventional undivided three-electrode cell, using an Autolab PGSTAT-30 potentiostat (Echo Chemie, Utrecht, the Netherlands), coupled to a microcomputer, interfaced by a GPES 4.9 software. UV-Vis spectra were obtained using a Hewlett Packard 8453 spectrophotometer.

Synthesis

Pterocarpanquinones **LQB-149** ((7*aS*,12*aS*)-9-nitro-7,7*a*-dihydro-5*H*-benzo[*g*]benzofuro[3,2-*c*]chromene-5,13(12*aH*)-dione), **150** ((7*aS*,12*aS*)-9-bromo-7,7*a*-dihydro-5*H*-benzo[*g*]benzofuro[3,2-*c*]chromene-5,13(12*aH*)-dione), **151** ((7*aS*,12*aS*)-9-chloro-7,7*a*-dihydro-5*H*-benzo[*g*]benzofuro[3,2-*c*]chromene-5,13(12*aH*)-dione) (Figure 1) were obtained from **LQB-118**,⁴ by electrophilic substitution, taking advantage of the high reactivity of E-ring for electrophilic aromatic substitution over the A-ring, which is deactivated due to the conjugation with the carbonyl groups of the quinone moiety (Figure 2).^{4,6} Their physicochemical parameters were herein reported.^{4,15} **LQB-149** should be kept refrigerated and under nitrogen to avoid decomposition.

Procedure for reductive thioalkylation of **LQB-150** by using hexanethiol as a nucleophile

A solution of **LQB-150** (8.0 mg, 0.0209 mmol) in 1:1 THF/MeOH (2.0 mL) and Trizma buffer (pH 7.4, 0.7 mL) was degassed for 15 min with dry, oxygen-free argon. Sodium dithionite (ca. 1 equiv.) was added to this solution to effect hydroquinone formation, followed by

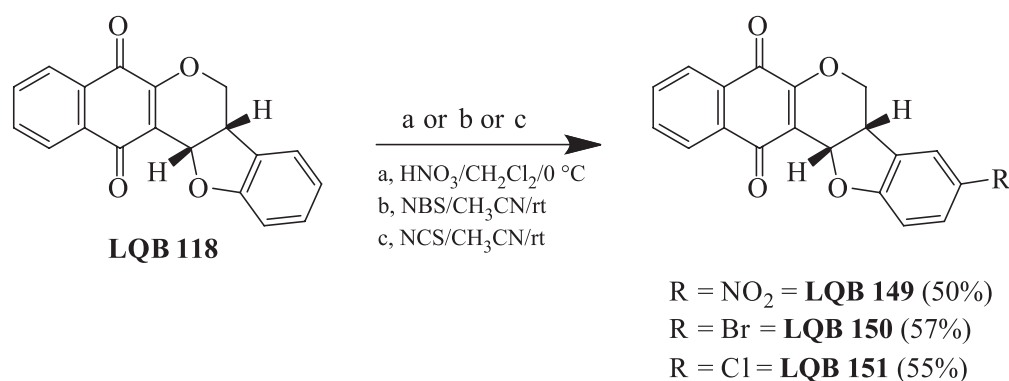


Figure 2. Synthesis of the pterocarpanquinones **LQBs-149**, **150** and **151** (adapted from reference 4).

addition of a solution of hexanethiol (4 equiv.) as the nucleophile in degassed 1:1 THF/MeOH (0.3 mL).^{4,5} The solution was stirred at room temperature (rt) under argon and the reaction was monitored periodically by using thin layer chromatography (TLC; eluent: Hex/EtOAc 7:3). Following extraction of the mixture with ethyl acetate (2 × 15 mL), the organic layer was washed with water (2 × 10 mL) and dried over anhydrous sodium sulfate. The solvent was removed under reduced pressure and the residue was purified by using column chromatography (silica gel, Hex/EtOAc 7.0:3.0), to afford compound **1** as a yellow solid (6.0 mg, 0.012 mmol, 57%).

¹H NMR (600 MHz, CDCl₃) δ 8.11 (dd, *J* 1.2, 7.2 Hz, 1H), 8.08 (dd, *J* 1.2, 7.2 Hz, 1H), 7.72 (ddd, *J* 1.2, 7.2, 7.2 Hz, 1H), 7.69 (ddd, *J* 1.2, 7.2, 7.2 Hz, 1H), 7.32 (d, *J* 2.4 Hz, 1H), 7.20 (dd, *J* 2.4, 8.4 Hz, 1H), 6.67 (d, *J* 8.4 Hz, 1H), 4.93 (dd, *J* 3.3, 12 Hz, 1H), 4.88 (dt, *J* 1.8, 12 Hz, 1H), 4.32 (s, 1H), 3.01-2.97 (m, 1H), 2.91-2.87 (m, 1H), 1.75-1.67 (m, 2H), 1.41-1.36 (m, 2H), 1.29-1.25 (m, 6H), 0.87 (t, *J* 7.2 Hz, 3H); ¹³C NMR (150 MHz, CDCl₃) δ 183.0, 179.1, 154.1, 152.2, 134.2, 133.3, 132.2, 131.4, 130.9, 129.7, 128.3, 126.6, 126.5, 120.1, 116.9, 113.3, 66.7, 37.1, 37.0, 33.7, 31.4, 29.8, 28.7, 22.6, 14.0.

Electrochemical studies

The electrochemical studies of halogenated and nitro-pterocarpanquinones, on glassy carbon electrode (GCE), were performed to evaluate their electrochemical behaviors, in aprotic medium, prior to the electrochemical studies with oxygen.

The working electrode was a GCE (*d* = 3 mm), the counter electrode was a Pt wire, and the reference electrode was an Ag|AgCl|Cl⁻ (saturated). Pt electrode (*d* = 1.6 mm) was also used as a working electrode. All electrodes were contained in a one-compartment electrochemical cell with a volumetric capacity of 5 mL. GCE was cleaned up by polishing with alumina on a polishing felt (BAS polishing kit). In CV experiments, the scan rate varied from 10 to 500 mV s⁻¹. For DPV measurements, the pulse amplitude was 50 mV, the pulse width was 70 ms and the scan rate was 5 mV s⁻¹. All experiments were performed at room temperature (25 ± 1 °C). Except when reported, all the CVs were displayed at scan rates of 100 mV s⁻¹.

Electrochemical reduction was performed in aprotic media (0.1 mol L⁻¹ DMF + TBAPF₆), at room temperature (25 ± 2 °C). Each compound (1 × 10⁻³ mol L⁻¹) was added to the supporting electrolyte, and the solution was deoxygenated with argon, before the CV measurements. The most representative potential range was from 0 to -2.2 V vs. Ag|AgCl|Cl⁻ (sat.).

To investigate the reactivity of **LQB-149**, **LQB-150** and **LQB-151** toward oxygen, electrochemical reduction in aprotic media (0.1 mol L⁻¹ DMF + TBAP) was performed in the presence and absence of oxygen. Oxygen was bubbled into the cell and its concentration monitored by an oxygen meter (Digimed DM-4). Cyclic voltammograms were recorded at different oxygen concentrations. The parameters analyzed were anodic shifts of the potential of the first reduction wave (E_{p1c}) and current increase at the same peak (I_{p1c}) or decrease of the correspondent anodic peak (I_{p1a}).¹⁶

Spectroelectrochemical experiments were performed on a thin-layer quartz electrochemical cell (path length 1 mm, BASi) with a three-electrode arrangement consisting of an optically transparent platinum minigrad as working electrode, a Pt wire as counter electrode and Ag|AgCl|Cl⁻ as reference. The cell was paired to the already described potentiostat and the spectra were obtained using a Hewlett Packard 8453 spectrophotometer.^{5,16} Measurements were carried out on deoxygenated solutions in 0.1 mol L⁻¹ DMF + TBAPF₆, at room temperature. The concentrations of **LQB-150** and **LQB-151** were 1.0 × 10⁻³ mol L⁻¹. The applied potentials were -0.6 and -1.1 V.

In the case of **LQB-149**, similar conditions were used, except the applied potentials, which were -0.5, -0.6 and -0.9 V vs. Ag|AgCl, Cl⁻.

Computational details

Full unconstrained geometry optimization and frequency calculations were carried out using the hybrid GGA B3LYP exchange-correlation functional.¹⁷ The triple zeta valence polarization (TZVP) basis set was used for describing H, C, O, N, Cl and Br atoms.¹⁸ The electronic spectra of all systems investigated were evaluated according to the time-dependent density functional theory (TD-DFT) formalism, using the ωB97DX exchange-functional,^{19,20} and TZVP basis set for all atoms. Solvent effects on electronic spectra calculations were treated using the linear response theory coupled with polarizable continuum model (LR-PCM),²¹ considering a dielectric constant equal to 37.219. All calculations were carried out using Gaussian09 program.²²

Results and Discussion

Electrochemistry

DMF was chosen as an aprotic organic solvent for electrochemical studies, because it can mimic the nonpolar environment in the cell, where lipid peroxidation, one of the causes of membrane fragmentation, normally occurs.²³

Non-aqueous solvents provide better models of a membrane environment, in which peroxidation processes take place, because both the superoxide radical anion and its conjugated acid, the hydroperoxyl radical, are unstable in water and other protic solvents, owing to their fast disproportionation.^{5,16} Additionally, in these conditions, single electron transfer occurs, generating the active semiquinone.²

As **LQB-118**, its halogenated derivatives, **LQB-150** and **151**, and nitrated one, **LQB-149**, have a *para*-naphthoquinone moiety, coupled to halogenated and nitrated aromatic rings, through non-conjugated pterocarpane-based spacers (Figure 1).

For **LQB-150** and **151**, the electrochemical profiles are complex, with at least 4 cathodic waves and a small, ill-defined shoulder (I'c), between waves Ic and IIc (Figures 3a-3d, Table 1). As shown before,⁵ the first wave corresponds to the formation of the semiquinone, while the second is related to the dianion of the generated hydroquinones. Additional waves refer to transient electrogenerated intermediates.⁵ Four anodic waves are present, which correspond to reduction peaks Ic (peak Ia), IIc (IIa and II'a) and IVc (IIIa) (Table 1).

As the electrochemical behaviors of **LQB-150** and **151** are very similar, detailed description will be provided for **LQB-150** (Figure 3, Table 1).

The first redox pair (Ic/Ia) is diffusion-controlled ($I_{p_{Ic}} \text{ vs. } \nu^{1/2}$) (Figure 3c), *quasi*-reversible, with $\Delta E_p = 76$ mV, $E_{p_{Ic}}$ does not modify with scan rate, I_{p_a}/I_{p_c} ca. 1 (Figure 3a, after reversion of potential at ca. -0.6 V), with the generation of a stable semiquinone. The second reduction process (IIc/IIa and II'a), corresponding to the formation of the hydroquinone dianion, is quite different from the first one, with a very low intensity anodic counterpart IIa. It also does not correspond to the usual behavior of quinones. Successive scans (Figure 3b) show a similar pattern as the first scan, with a slight increase of peak I'c. Upon potential inversion (Figure 3a), its correspondence to the peak assigned as II'a is observed. This behavior comes from its higher basicity, and cleavage of the pterocarpane moiety, originating a phenolate, which oxidation occurs at II'a. This behavior was reported recently for the standard compound (**LQB-118**), through electrochemical reduction,⁵ similarly to the homogenous chemical reaction.

It is well-known that electron-withdrawing groups, in conjugation to the electroactive group, facilitates its reduction, with an anodic shift in its reduction potential.¹¹ That is the case for **LQB-149**, with two electroactive groups: the quinone and the aromatic nitro group. The comparison between Figures 3a, 3d and 3e reveals different redox profiles.

For **LQB-149**, it is evident the presence of five reduction waves (Ic-Vc) and four ill-defined oxidation ones (Figure 3e). The first wave (Ic = -0.579 V) is diffusional-controlled ($I_{p_{Ic}} \text{ vs. } \nu^{1/2}$), similar to the others, with a slightly more positive potential, once there is no conjugation between the redox groups. It represents a *quasi*-reversible process, $\Delta E_p = 89$ mV, $E_{p_{Ic}}$ does not modify with scan rate. The second wave is broad (IIc = -0.787 V), presents an anodic counterpart, and is related to the reduction of the nitro group, probably generating a biradical-dianion, reported before for *ortho*-quinones substituted with non-conjugated nitroanilines.¹² Waves IIIc and IVc are similar to the other compounds and the last reduction wave, Vc, irreversible in terms of the nature of electron transfer ($V_c = -2.116$ V), with a higher current intensity, is related to the further reduction of the nitro radical anion.^{11,12}

Further redox information, under the same condition, can be obtained through the use of DPV, once it is a more sensitive electrochemical technique.

The comparison of redox profiles is better visualized in Figure 4, where the three compounds are compared with the unsubstituted one, **LQB-118**.⁵ Due to the difference in scan rate, DPV can be slightly different from CV.

As the standard compound (**LQB-118**), the two halogenated compounds had shown 4 main waves, at similar potentials. The presence of shoulders between Ic and IIc (Figure 4) occurs, when a C-X (X = halogen) bonding is present and the reason of their presence is still uncertain.

LQB-149 is clearly different, represented by five main waves, the last one, very broad. As already shown by CV, waves Ic and IIc correspond to the sequential monoelectronic reduction of the quinone and nitro functionalities, and the others related to the reduction of the dianion diradical, to the tri-anion-radical, which suffers cleavage, as evidenced for the other compounds. Wave Vc (broad), as shown before in CV, is related to an extended reduction of the nitro radical anion.

In situ UV-Vis spectroelectrochemistry in aprotic medium

This technique is useful for giving detailed structural information about the compounds obtained from heterogeneous electron transfer reactions.^{5,14} The changes in radical intermediates (semiquinones), in 0.1 mol L^{-1} DMF + TBABF₄, originated at the first reduction potential, and final reduced species, can be monitored by electronic transitions, using *in situ* UV-Vis spectroelectrochemical experiments, in a kinetic mode for collecting spectra. Table 1 lists all the reduction potentials (in V) and data on UV-Vis (nm), before and after reduction.

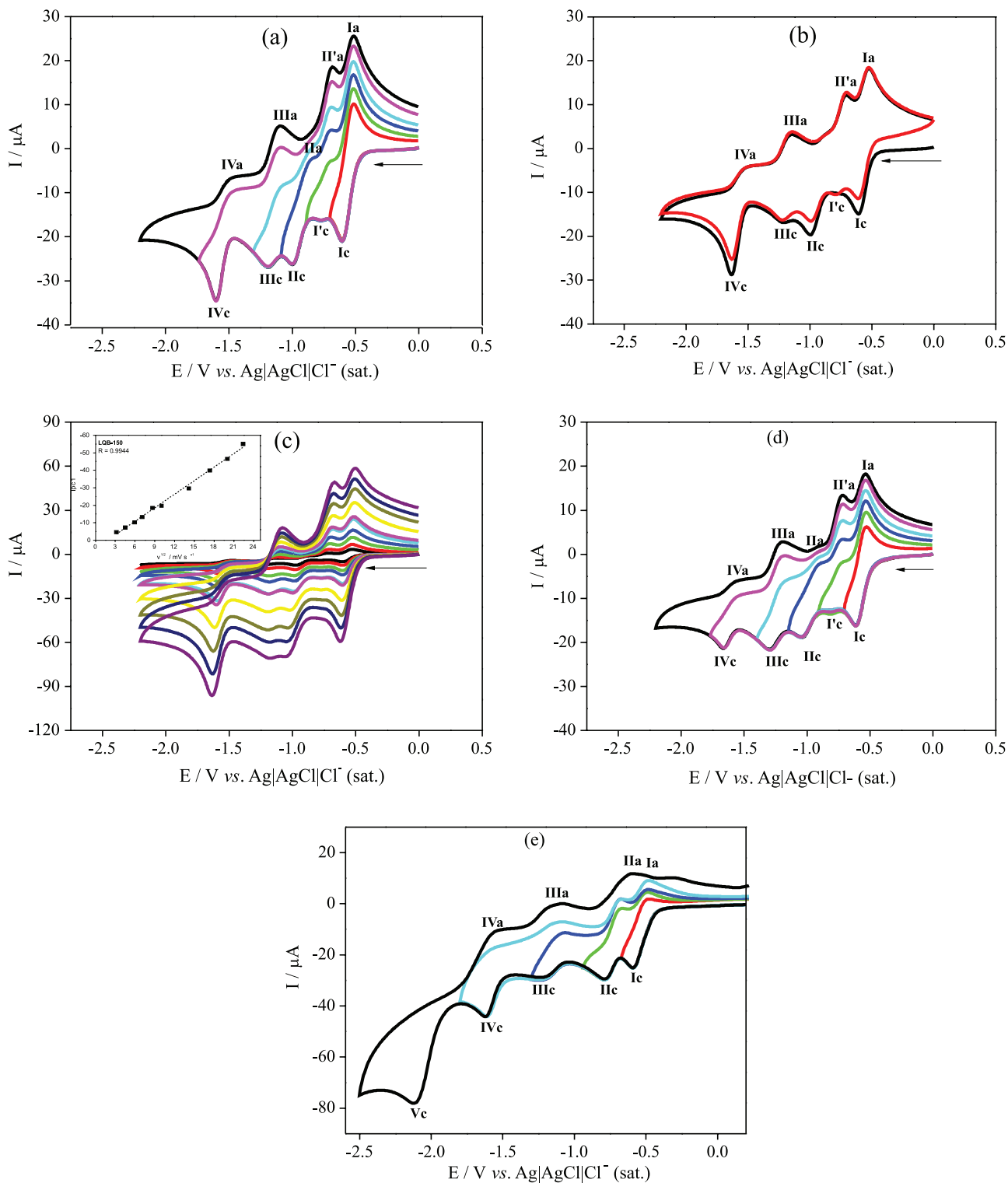


Figure 3. Cyclic voltammetry (CV) of compounds (1 mmol L^{-1}) in DMF + TBAPF₆ (0.1 mol L^{-1}), glassy carbon electrode, vs. Ag/AgCl, Cl⁻, cathodic direction, $v = 100 \text{ mV s}^{-1}$. (a) **LQB-150**, different inversion potentials; (b) **LQB-150**, successive CVs; black line: scan 1, red line: scan 2; (c) **LQB-150**, CVs at different scan rates of 20, 40, 60, 80, 100, 150, and 200 mV s^{-1} . The inset shows the linear increasing of the redox peak current depends on increasing the square root of the scan rate; (d) **LQB-151**, different inversion potentials; (e) **LQB-149**, different inversion potentials.

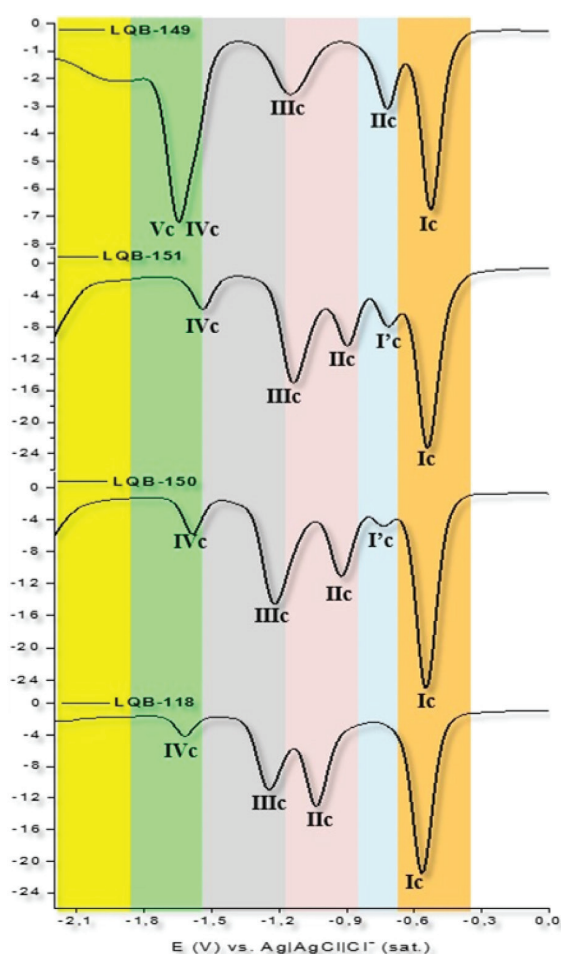
As aforementioned, there is similarity in electrochemical behavior for the standard compound, **LQB-118**, already reported,⁵ and its halogenated derivatives. Before reduction,

LQB-150 and **151** exhibit two main waves, related to π - π^* and n - π^* transitions, at 280 and 330 nm (Table 1, Figure 5). During the cathodic scan, in the potential range of 0 up

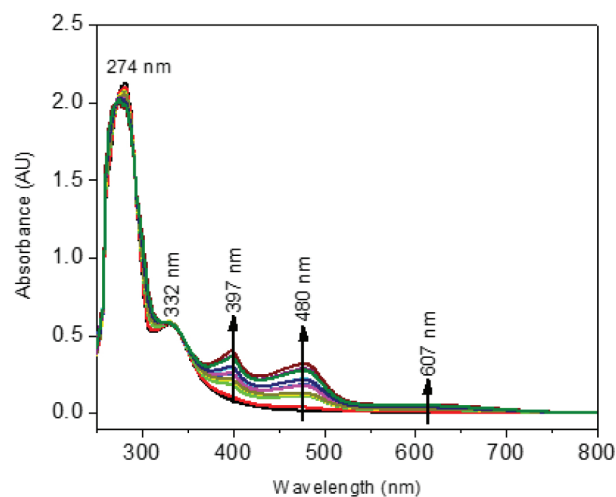
Table 1. Major electrochemical parameters (V) in CV and DPV of **LQB-149** ($c = 1 \text{ mmol L}^{-1}$), **LQB-150** and **LQB-151**, in DMF + TBAPF₆, 0.1 mol L^{-1} , $v = 100 \text{ mV s}^{-1}$

Compound	Cyclic voltammetry (CV)										Differential pulse voltammetry (DPV)					UV-visible				
	Ep _{Ic} /	Ep _{IIc} /	Ep _{IIIc} /	Ep _{IVc} /	Ep _{Vc} /	Ep _{IIa} /	Ep _{IIIa} /	Ep _{IVa} /	Ep _{Va} /	Ep _{VIa} /	Ep _{Ic} /	Ep _{IIc} /	Ep _{IIIc} /	Ep _{IVc} /	Ep _{Vc} /	λ _{initial} /	New bands after reduction			
	V	V	V	V	V	V	V	V	V	V	V	V	V	V	nm	(λ) / nm				
LQB-118	-0.624	-1.119	-1.303	-1.688	-	-0.548	-0.757	-0.992	-1.211	-1.564	-0.567	-1.036	-1.251	-1.615	-	276	331	400	470	600
LQB-149	-0.579	-0.787	-1.233	-1.608	-2.116	-0.490	-	-0.607	-1.125	-	-0.532	-0.721	-1.146	-1.649	-1.952	279	326	432	-	-
LQB-150	-0.592	-0.792	-0.996	-1.194	-1.595	-0.516	-	-0.684	-	-	-0.547	-0.923	-1.216	-1.584	-	-	-	-	-	-
LQB-151	-0.602	-0.810	-1.043	-1.294	-1.668	-0.532	-	-0.717	-	-	-0.542	-0.899	-1.133	-1.542	-	280	330	397	480	607

Ep_{Ic}: potential of the cathodic wave Ic; Ep_{IIc}: potential of the cathodic wave IIc; Ep_{IIIc}: potential of the cathodic wave IIIc; Ep_{IVc}: potential of the cathodic wave IVc; Ep_{Vc}: potential of the cathodic wave Vc; Ep_{IIa}: potential of the anodic wave II'a; Ep_{IIIa}: potential of the anodic wave IIIa; Ep_{IVa}: potential of the anodic wave IVa.

**Figure 4.** Differential pulse voltammograms for the studied compounds, **LQB-149**, **150**, **151**, together with **LQB-118** ($c = 1 \text{ mmol L}^{-1}$), in DMF + TBAPF₆ (0.1 mol L^{-1}), glassy carbon electrode, $v = 5 \text{ mV s}^{-1}$.

to -1.5 V , significant modifications in the UV-Vis spectra occurred, indicative of structural changes. As shown in Figure 5, the band at 280 nm is blue-shifted (from 280 to 274 nm). New bands have appeared at 397 and 480 nm , followed by a low-intensity one at 607 nm (Table 1). The last bands were assigned to the absorption of the electrogenerated quinonemethide (QM).^{5,24-27}

**Figure 5.** *In situ* UV-Vis spectra in 0.1 mol L^{-1} DMF + TBAPF₆, obtained in an optically transparent electrochemical cell, optical path of 1 mm of **LQB-151** ($c = 1.0 \text{ mmol L}^{-1}$), Pt electrode. UV-Vis spectrum obtained after applying the second wave potential, during 240 s . Initial waves at 280 and 330 nm are from non-reduced **LQB-151**.

To get additional evidences for the occurrence of the putative quinonemethide, derived from **LQB-151**, the reduction was held, into the UV cell, in the presence of electrochemically/UV-Vis transparent hexanethiol (Figure 6). A potential of -1.1 V , relative to the second reduction wave, was applied. For the first 180 s , the absorption bands of the QM (Figure 6, pink line) were evidenced. Soon after this contact time, a significant decrease on absorbance of these bands were observed (Figure 6, green line at 600 s), indicative of the QM capture, through thioalkylation, as confirmed as follows and similarly to reported behavior of **LQB-118**, by homogeneous chemical reaction.⁵

The spectroelectrochemistry of **LQB-150** was also held and had shown similar results as **LQB-151** (figure not shown). In order to get a more definite proof of the QM capture, envisaged in the spectroelectrochemical experiment (Figure 6), a chemical reduction by sodium dithionite was performed in the presence of hexanethiol

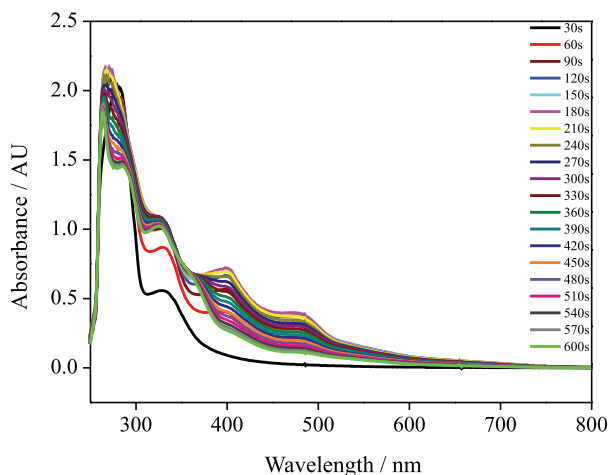


Figure 6. Successive UV-Vis spectra of **LQB-151** ($c = 1.0 \text{ mmol L}^{-1}$), in 0.1 mol L^{-1} DMF + TBAPF₆, in a quartz cell, optical path of 1 mm, applying a potential of -1.1 V , during 30 up to 600 s, in the presence of UV-Vis transparent hexanethiol.

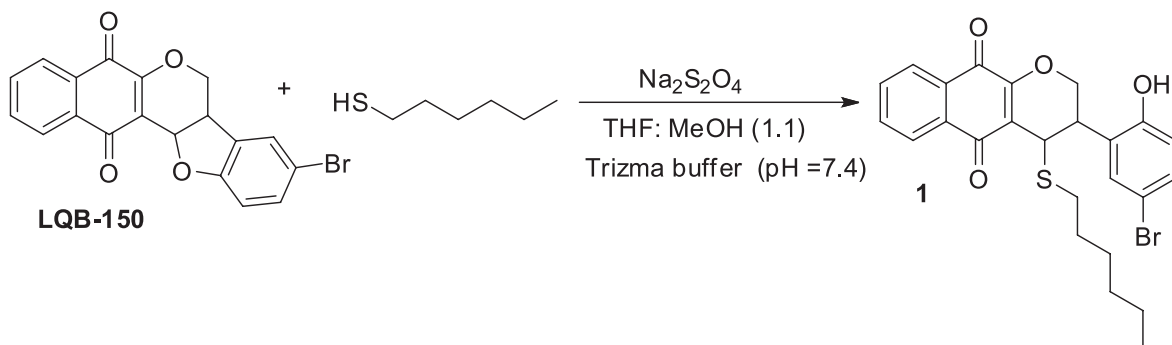


Figure 7. Reductive thioalkylation of **LQB-150**.

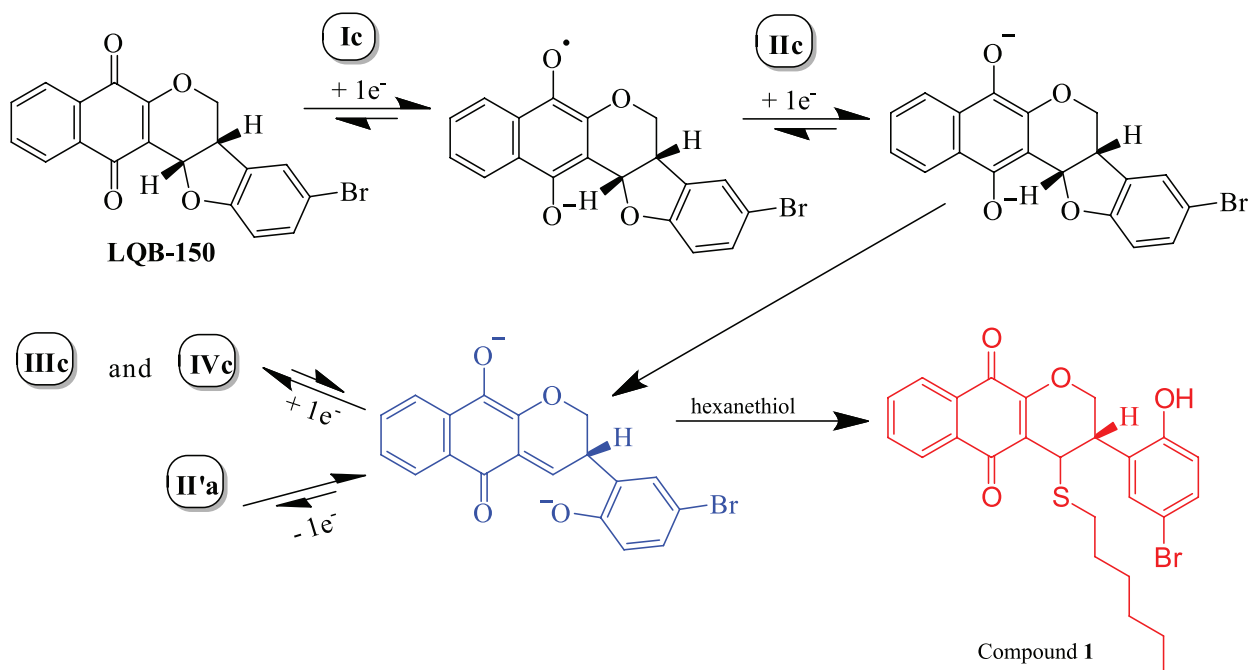


Figure 8. Possible reduction mechanism for the reduction of **LQB-150**. Protonation steps were not included. In blue, the generated quinonemethide (QM), able to react with hexanethiol, leading to the new compound **1** (red).

(Figure 7), using **LQB-150**. A novel thiosubstituted compound **1** was obtained and characterized by ¹H and ¹³C NMR (see Figures S2 and S3, Supplementary Information (SI) section).

Combined data allowed to build the following scheme for the electrochemical reduction of **LQB-150** (Figure 8).

For **LQB-149**, the spectroelectrochemical experiments were performed under the same conditions (DMF + TBAPF₆, 0.1 mol L^{-1}). The UV-Vis spectra showed a different pattern when compared with **LQB-151** and reported **LQB-118**.⁵

Before reduction, **LQB-149** (nitroderivative) was characterized by transitions $\pi-\pi^*$ and $n-\pi^*$ at 279 and 326 nm (Table 1, Figure 9, red line). After applying the potential of -0.9 V , for 240 or 500 s, the absorbance of the last bands decreased, with the appearance of a new one, at 432 nm (Figure 9). It is useful to remark that the absorption

bands, associated to QM, were not present, suggesting a different reduction outcome. For **LQB-149**, there is, at the second potential wave, the reduction of the nitro group, giving the nitro radical anion (Figure 10).

The presence of the radical anion nitro was earlier

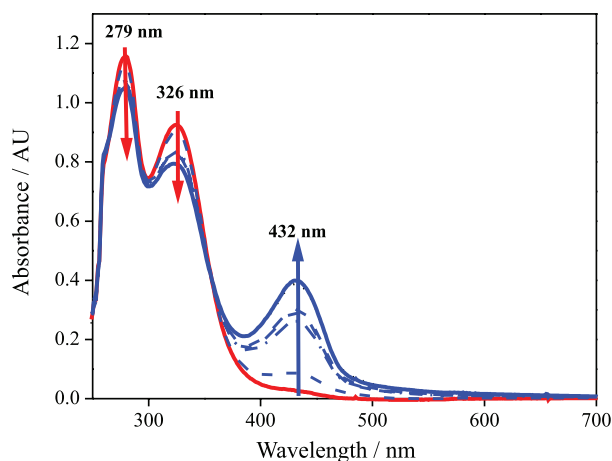


Figure 9. *In situ* UV-Vis spectra in 0.1 mol L⁻¹ DMF + TBAPF₆, obtained in an optically transparent electrochemical cell, optical path of 1 mm of **LQB-149** (*c* = 1.0 mmol L⁻¹), Pt electrode. The initial spectrum is represented by two bands at 279 and 326 nm (curve in red), followed by UV-Vis spectrum obtained after applying close to the second wave potential (-0.9 V), during 240 s (curve in blue).

observed for polinitrocalix[4]arenes and several other nitroaromatics.²⁸ A new absorption UV-Vis band with a maximum at 451 nm is formed, as a consequence of reductive electrolysis monitored by coulometry, under the same conditions (DMF + Bu₄NPF₆).²⁸

Based on the above facts, the reduction mechanism for **LQB-149** was proposed as shown in Figure 10.

Electrochemical studies in the presence of oxygen

As already reported, one of the proposed molecular mechanism of action for pterocarpanquinones is the bioreduction, which in presence of oxygen, leads to the release of ROS, assigned as electron transfer/oxidative stress (ET/OS),^{1,2,5} definitely recognized as an important mechanism against cancer cells and parasites. The interaction of quinones with oxygen, including from **LQB-118**,⁵ have already been reported and presented some positive trends, revealed when electroactivity was compared with biological parameters.^{2,5}

Based on the relevant role of redox cycling of quinones and nitroquinones, in the presence of oxygen, **LQB-149**, **LQB-150** and **151** were also analyzed towards oxygen, in aprotic media, as explained before. **LQB-118** was included for comparison purposes. **LQB-151** was chosen for a

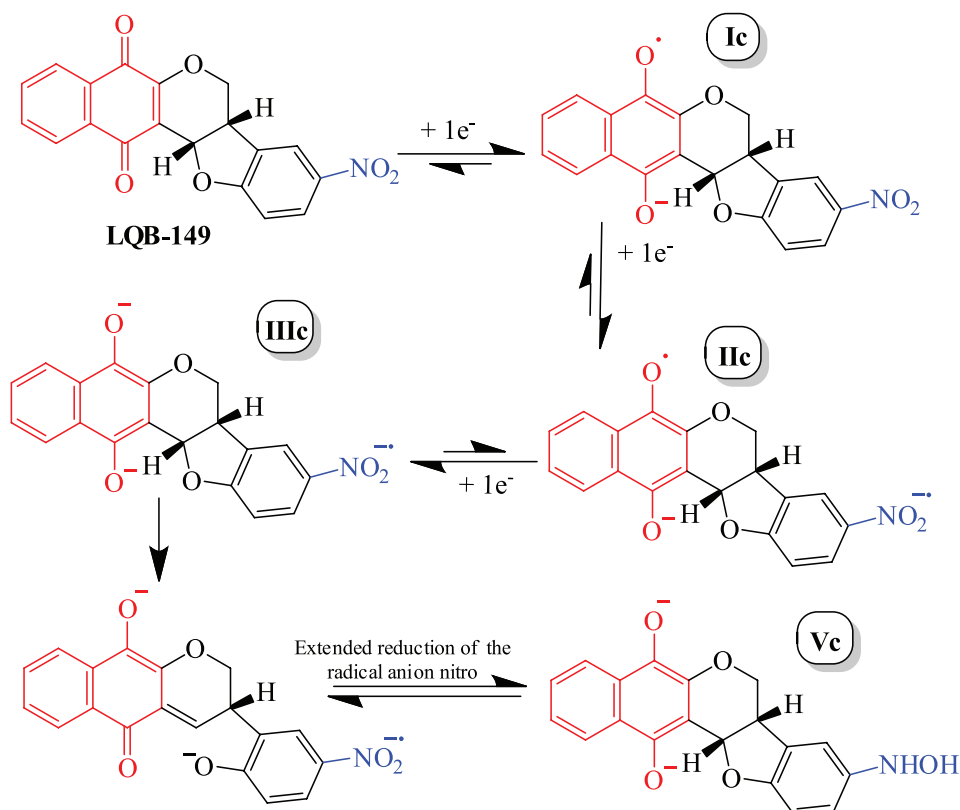


Figure 10. Proposed mechanism for **LQB-149**. In red, reduction of the quinone moiety, and in blue, the reduction of the nitro group. The protonation steps were not included.

more complete study, as shown in Figure 10. Oxygen is electroactive (Figure 11, in blue). Upon addition of oxygen, in the electrochemical cell, in the presence of **LQB-151** (CV in black), there is a slight anodic shift of the first reduction potential ($E_{p_{ic}}$) and the increase of respective current ($I_{p_{ic}}$), diagnostic features for oxygen interaction (CV in red). The addition of oxygen also leads to the constant regeneration of the initial quinone, resulting in the disappearance of the sequential reduction peaks (CV in red). It is also useful to note that the reaction with O_2 is reversible and does not cause structural modification. This was proved by deaeration with nitrogen and recovery of the original redox profile of **LQB-151** (figure not shown).

The reactivities of these 3 quinones toward oxygen are displayed in Figure 12, where the diagnostic figures appeared, represented by an increase of the current of the first cathodic wave and decrease of the corresponding anodic one. The apparent rate constant, obtained as already shown,^{5,17} are similar, with a lower value for **LQB-149** (Figure 12):¹⁷

$$\begin{aligned} \text{LQB-118 (0.17 s}^{-1}) \sim \text{LQB-150 (0.13 s}^{-1}) = \\ \text{LQB-151 (0.13 s}^{-1}) > \text{LQB-149 (0.08 s}^{-1}) \end{aligned} \quad (1)$$

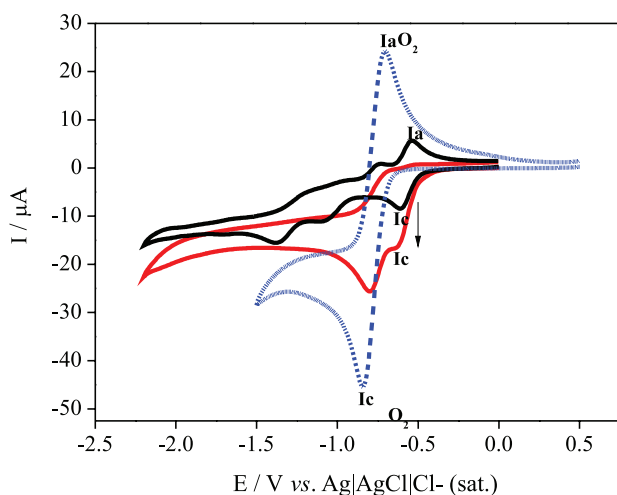


Figure 11. Cyclic voltammograms of **LQB-151**, in DMF + TBAP (0.1 mol L⁻¹), GCE, in absence of oxygen (black) and in the presence of oxygen (red), $v = 50 \text{ mV s}^{-1}$. In blue, oxygen in DMF + TBAPF₆.

Present results suggest the generation of ROS, important and proved mechanism for the cytotoxic and antiparasitic activities of these compounds.^{5,16}

Computational studies

DFT and TD-DFT calculations were carried out in order to get additional information regarding the nature of the UV-Vis spectra of the compounds studied (**LQB-118**,

LQB-149, **LQB-150** and **LQB-151**). Figure 13 displays the UV-Vis spectra calculated at $\omega\text{B97DX/TZVP(LR-PCM)}$ level of theory.

According to current spectroelectrochemical results herein presented (Table 1, Figures 5, 6 and 9), the UV-Vis spectra of **LQB-118**, **LQB-149**, **LQB-150** and **LQB-151** before reduction are characterized by two well-defined bands, one at 276-280 nm and another between 326-331 nm. The results presented in Figure 13 shows that the results obtained at $\omega\text{B97DX/TZVP(LR-PCM)}$ level of theory are in good agreement with these experimental values. In relation to **LQB-118** (curve in black), for instance, the calculated values of ca. 265.0 nm for the first band and ca. 300.0 nm for the second one is in close agreement with values of 276.0 and 331.0 nm observed experimentally. Similar agreement was also obtained if we compare the calculated values (curve in red) of ca. 285.0 and 314 nm with experimental values of 279 and 326 nm determined for **LQB-149**. For **LQB-150** (curve in blue), the calculated values of the first and second absorption bands were ca. 284.0 and 317.0 nm. The theoretical results are also in line with the slight bathochromic effect observed experimentally for the first absorption band, when one of the aromatic rings of **LQB-118** is modified by substitution of a hydrogen atom for $-\text{NO}_2$, $-\text{Br}$ and $-\text{Cl}$.

In order to understand the nature of the electronic transitions responsible for the bands observed in the investigated systems, we carried out an analysis of the Kohn-Sham molecular orbitals in these transitions. Figure 14 shows the Kohn-Sham molecular orbitals involved in the electronic transitions in **LQB-118**.

According to Figure 14, the two absorption bands observed in **LQB-118** are essentially characterized by electronic transition of the type $\pi-\pi^*$ and $n-\pi^*$. As can also be seen in Figure 14, the atoms of the quinone moiety contribute more effectively for the molecular orbitals related with the electronic transitions of the absorption bands at 265.0 and 330.0 nm. On the other hand, as shown in Figure 15, the absorption bands at 284.0 and 314 nm calculated for **LQB-149** are mostly characterized by electronic transitions involving molecular orbitals composed essentially by NO_2 -functionalized aromatic ring adjacent to the quinone moiety. The comparison of the Kohn-Sham molecular orbitals of **LQB-118** and **LQB-149** shows clearly how the substitution with $-\text{NO}_2$ affects the electronic structure of **LQB-118**.

In order to provide additional support for the mechanism proposed in this paper for the reduction process of **LQB-118**, **LQB-149**, **LQB-150** and **LQB-151**, we calculated at $\omega\text{B97DX/TZVP(LR-PCM)}$ level the UV-Vis

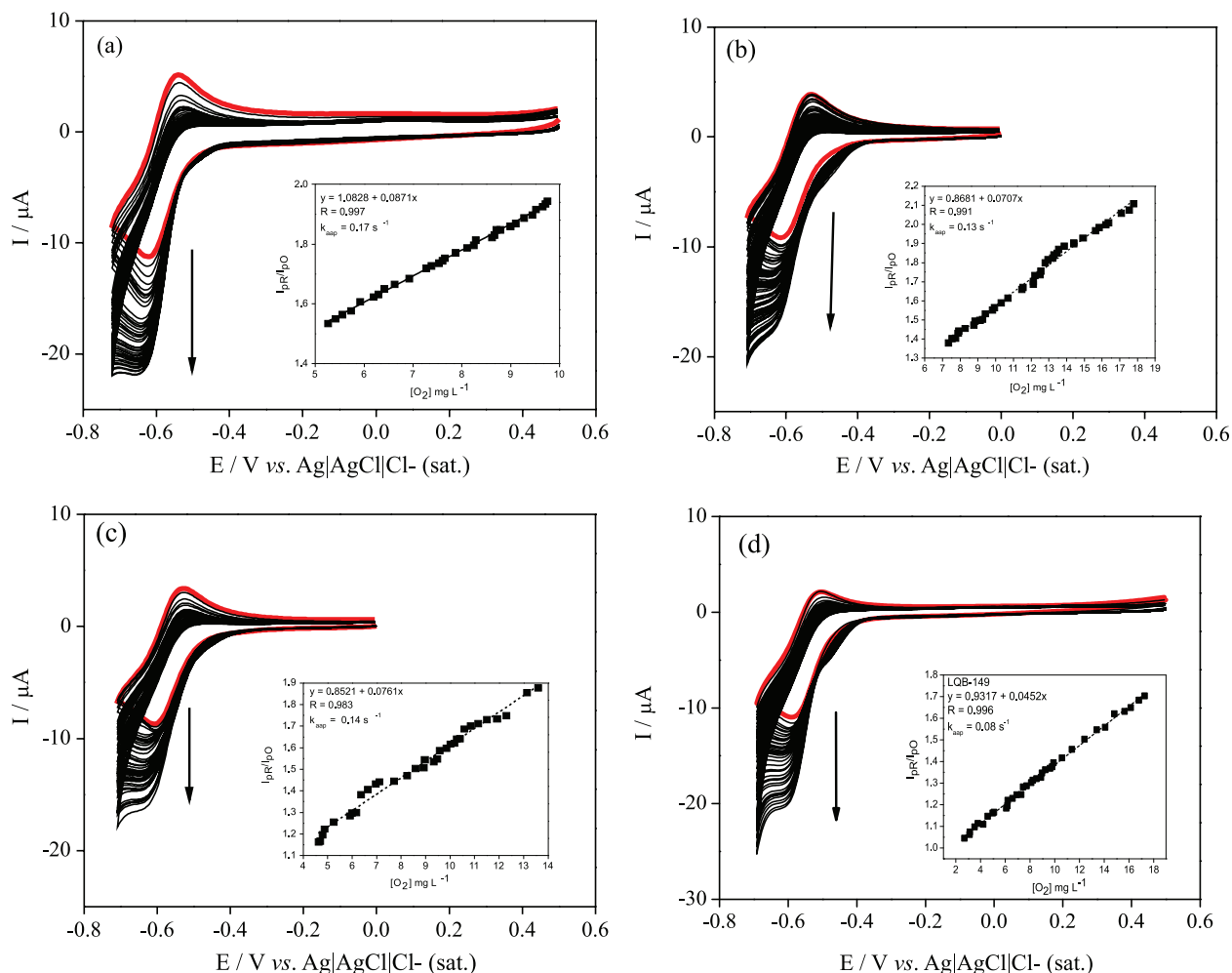


Figure 12. Cyclic voltammograms for the studied compounds in DMF + TBAP (0.1 mol L⁻¹), GCE, in absence of oxygen (red) and in the presence of different concentrations of oxygen, $v = 50 \text{ mV s}^{-1}$. (a) **LQB-118**; (b) **LQB-150**; (c) **LQB-151**; (d) **LQB-149**. Inset: linear graphs of I_{pr} / I_{po} in function of oxygen concentration, to obtain the apparent constant of reactivity toward oxygen.

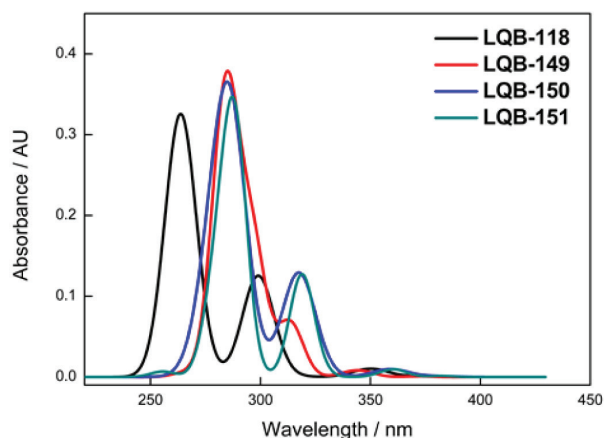


Figure 13. Electronic spectra calculated at $\omega\text{B97DX/TZVP(LR-PCM)}$ level for **LQB-118**, **LQB-149**, **LQB-150** and **LQB-151** molecules.

spectrum of the reduced form of these compounds generated via successive reduction steps and compared with experimental results. Figure 16 shows the calculated UV-Vis spectra of the **LQB-118**, **LQB-149**, **LQB-150** and

LQB-151 and their reduced forms, **IIIc**, followed by the analysis of the Kohn-Sham molecular orbitals involved in the electronic transitions.

Analyzing the results presented in Figure 16, it is possible to note some relationship between theory and experiment. For instance, the spectroelectrochemical study revealed that the reduction process of **LQB-149** molecule is characterized by the appearance of a new absorption band at 432 nm. Our computational results, shown in Figure 16 (curve in red), predict the appearance of an intense band at around 406 nm, whose Kohn-Sham molecular orbitals analysis (Figure 17) indicates to be related to an electronic transition involving essentially the quinone ring portion and the NO_2 -functionalized aromatic ring. The computational results of Figure 16 also show, as observed experimentally, that the UV-Vis spectrum profile of the reduced form of **LQB-149** has a pattern different from the other pterocarpanquinones, herein investigated.

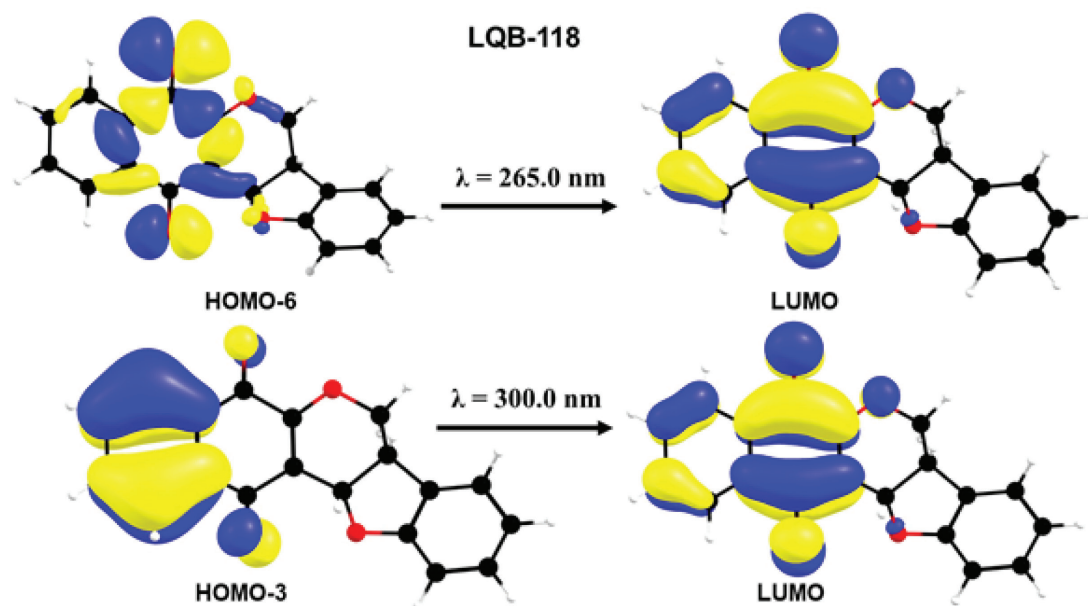


Figure 14. The Kohn-Sham molecular orbitals involved electronic transitions related with the absorption bands in LQB-118.

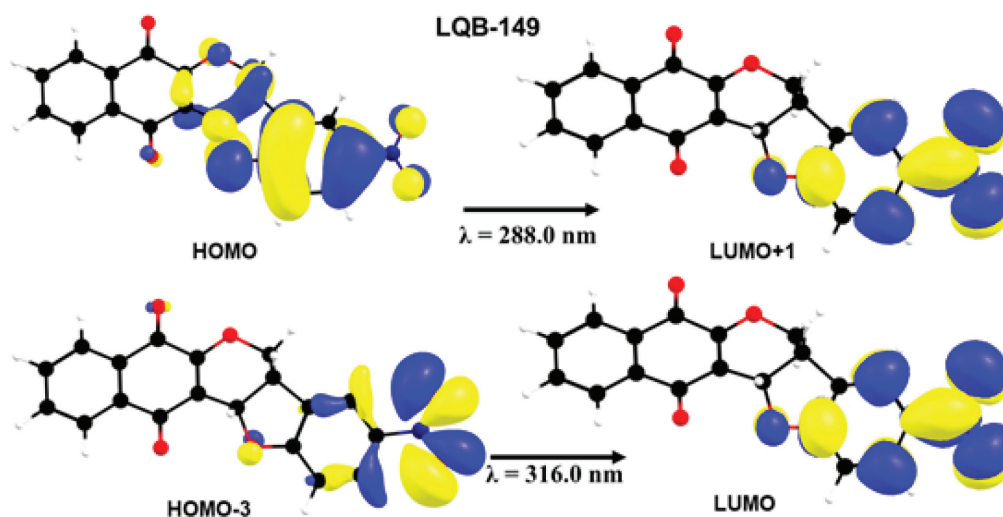


Figure 15. The Kohn-Sham molecular orbitals involved electronic transitions related with the absorption bands in LQB-149 molecule.

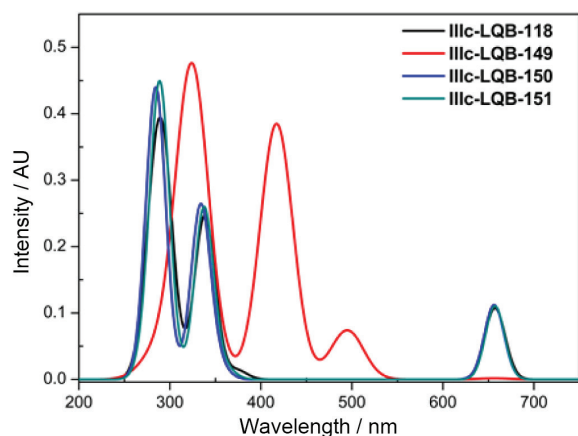


Figure 16. Electronic spectra calculated at ω B97DX/TZVP(LR-PCM) level for reduced forms of the pterocarpanquinones studied.

Also, in line with part of experimental results, our computational results obtained at ω B97DX/TZVP(LR-PCM) level of theory, predict the appearance of a low intensity absorption band above 600.0 nm for reduced form of LQB-118, LQB-150 and LQB-151 compounds. Kohn-Sham molecular orbitals analysis shows that this absorption band is related with electronic transitions involving essentially the quinone portion of these molecules (Figure S1, SI section). It is worth noting that according to our theoretical results, the functionalization of aromatic ring in LQB-118 (curve in black), with the halogens Cl and Br (curves in blue and dark cyan) does not provide significant changes in the profile of their reduced form UV-Vis spectra. Similar

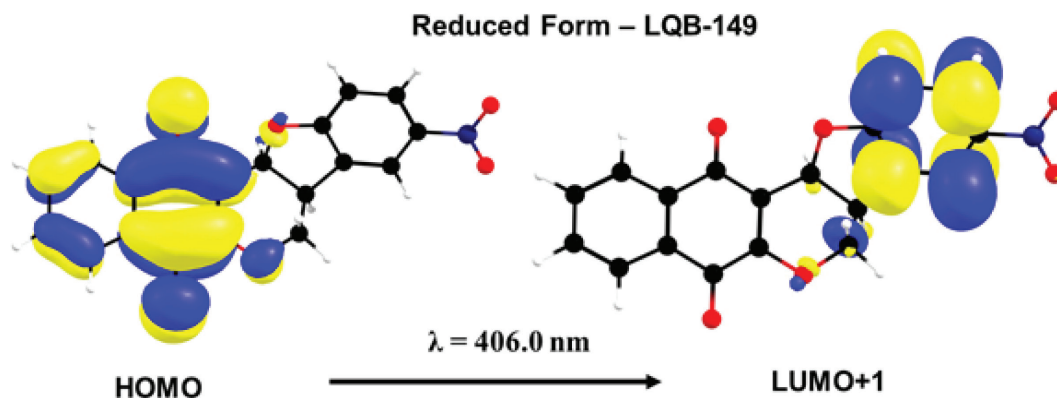


Figure 17. The Kohn-Sham molecular orbitals involved electronic transitions related with the absorption band at 400.0 nm in reduced form of **LQB-149** molecule.

behavior was also observed experimentally. Nevertheless, contrary to what has been observed experimentally, our calculations do not reveal appearance of the absorption bands at 400 and 470 nm measured for reduced forms of **LQB-118**, **LQB-150** and **LQB-151**. It is well known that the quality of DFT and TD-DFT results is quite dependent on factors as nature of the exchange-correlation functional and basis set,²⁹ so that the establishment of an accurate methodology requires the performance of systematic studies. This type of analysis is not the main goal of the current work, and these referred issues will be evaluated in future work. In any case, the ω B97DX/TZVP(LR-PCM) results obtained here can be interpreted in a semi-quantitative way and have provided additional support for proposed mechanism for reduction of pterocarpanquinones.

Conclusions

The electrochemical results have confirmed the difference in behavior of the modified pterocarpanquinones: the halogenated ones follow the behavior of **LQB-118**, while the nitroderivative presents a reduction profile compatible with the generation, at the second reduction potential, of a dianion-diradical, which can explain, in part, its higher cytotoxicity towards normal cells, decreasing its selectivity index. However, this special feature allows **LQB-149** to be an effective parasitocidal compound. We may affirm that electrochemical methods contribute significantly to the definition of the mechanism of molecular action of drugs, particularly when quinonemethides (QM) are involved as electrogenerated intermediates or in the case of the release of reactive oxygen species (ROS), among other possibilities. Overall, electrochemical techniques appear well adapted to explore redox pathways *in vitro*, which can be related to *in vivo* studies.

Supplementary Information

Supplementary data (DFT and NMR) are available free of charge at <http://jbcs.sbc.org.br> as PDF file.

Acknowledgments

The authors wish to thank the Brazilian financial agencies: CNPq, CAPES, FAPAL, FAPERJ and INCT in Bioanalytics (FAPESP grant No. 2014/50867-3 and CNPq grant No. 465389/2014-7, 458114/2014-6). The authors also thank the LQTC (Laboratório de Química Teórica e Computacional, Universidade Federal de Pernambuco) for the computational resources used to perform the calculations. They also acknowledge the excellent revision done by reviewers of the present manuscript.

References

- Kumagai, Y.; Shinkai, Y.; Miura, T.; Cho, A. K.; *Annu. Rev. Pharmacol. Toxicol.* **2012**, *52*, 221; Colucci, M. A.; Moody, C. J.; Couch, G. D.; *Org. Biomol. Chem.* **2008**, *6*, 637; Ma, W.; Long, Y.-T.; *Chem. Soc. Rev.* **2014**, *43*, 30; Bolton, J. L.; Trush, M. A.; Penning, T. M.; Dryhurst, G.; Monks, T. J.; *Chem. Res. Toxicol.* **2000**, *13*, 135; Bolton, J. L.; Dunlap, T.; *Chem. Res. Toxicol.* **2017**, *30*, 13.
- Hillard, E. A.; de Abreu, F. C.; Ferreira, D. C. M.; Jaouen, G.; Goulart, M. O. F.; Amatore, C.; *Chem. Commun.* **2008**, 2612; Kovacic, P.; Somanathan, S.; *Anti-Cancer Agents Med. Chem.* **2011**, *11*, 658; Santini, C.; Pellei, M.; Gandin, V.; Porchia, M.; Tisato, F.; Marzano, C.; *Chem. Rev.* **2014**, *114*, 815.
- Klotz, L.-O.; Hou, X.; Jacob, C.; *Molecules* **2014**, *19*, 14902.
- Netto, C. D.; da Silva, A. J. M.; Salustiano, E. J. S.; Bacelar, T. S.; Riça, I. G.; Cavalcante, M. C. M.; Rumjanek, V. M.; Costa, P. R. R.; *Bioorg. Med. Chem.* **2010**, *18*, 1610.
- Silva, T. L.; Ferreira, F. R.; Vasconcelos, C. C.; da Silva, R. C.;

- Lima, D. J. P.; Costa, P. R. R.; Netto, C. D.; Goulart, M. O. F.; *ChemElectroChem* **2016**, *3*, 2252.
6. Martino, T.; Kudrolli, T. A.; Kumar, B.; Salviano, I.; Mencialha, A.; Coelho, M. G. P.; Justo, G.; Costa, P. R. R.; Sabino, K. C. C.; Lupold, S. E.; *Prostate* **2018**, *78*, 140.
7. Silva, K. L.; Souza, P. S.; Costa, P. R. R.; Maia, R. C.; *Clin. Cancer Res.* **2015**, *21*, A51.
8. da Silva, L. L. R.; Portes, J. A.; de Araújo, M. H.; Silva, J. L. S.; Rennó, M. N.; Netto, C. D.; da Silva, A. J. M.; Costa, P. R. R.; de Souza, W.; Seabra, S. H.; DaMatta, R. A.; *Parasitol. Int.* **2015**, *64*, 622.
9. Wondrak, G. T.; *Antioxid. Redox Signaling* **2009**, *11*, 3013; McKeown, S. R.; Coweny, R. L.; Williamsy, K. J.; *Clin. Oncol.* **2007**, *19*, 427; Rahman, M. H.; Bal, M. K.; Jones, A. M.; *ChemElectroChem* **2019**, *6*, DOI: 10.1002/celc.201900117.
10. Ribeiro, G. A.; Cunha-Junior, E. F.; Pinheiro, R. O.; da-Silva, S. A. G.; Canto-Cavalheiro, M. M.; da Silva, A. J. M.; Costa, P. R. R.; Netto, C. D.; Melo, R. C. N.; Almeida-Amaral, E. E.; Torres-Santos, E. C.; *J. Antimicrob. Chemother.* **2013**, *68*, 789.
11. Nepali, K.; Lee, H.-Y.; Liou, J.-P.; *J. Med. Chem.* **2019**, *62*, 2851; Hammerich, O. In *Organic Electrochemistry*; Hammerich, O.; Speiser, B., eds.; CRC Press: Boca Raton, 2016, p. 1149 (and included references).
12. Armendáriz-Vidales, G.; Hernández-Muñoz, L. S.; González, F. J.; de Souza, A. A.; de Abreu, F. C.; Jardim, G. A. M.; da Silva Júnior, E. N.; Goulart, M. O. F.; Frontana, C.; *J. Org. Chem.* **2014**, *79*, 5201.
13. Saveant, J. M.; *Elements of Molecular and Biomolecular Electrochemistry: An Electrochemical Approach to Electron Transfer Chemistry*; Wiley: New York, 2006; Andrieux, C. P.; Le Gorand, A.; Saveant, J. M.; *J. Am. Chem. Soc.* **1992**, *114*, 6892; Gennaro, A.; Isse, A. A.; Bianchi, C. L.; Mussini, P. R.; Rossi, M.; *Electrochem. Commun.* **2009**, *11*, 1932; Jardim, G. A. M.; Silva, T. L.; Goulart, M. O. F.; de Simone, C. A.; Barbosa, J. M. C.; Salomão, K.; de Castro, S. L.; Bower, J. F.; da Silva Júnior, E. N.; *Eur. J. Med. Chem.* **2017**, *136*, 406.
14. Ma, W.; Zhou, H.; Ying, Y.; Li, D.; Chen, G.; Long, Y.; Chen, H.; *Tetrahedron* **2011**, *67*, 5990; Costentin, C.; *Chem. Rev.* **2008**, *108*, 2145; Rapta, P.; Dmitrieva, E.; Alexey, A.; Popov, A. A.; Dunsch, L. In *Organic Electrochemistry*; Hammerich, O.; Speiser, B., eds.; CRC Press: Boca Raton, 2016, p. 169 (and included references).
15. de Moraes, P. F.; Gaspar, F. V.; Borges, R. H. F.; Netto, C. D.; Leão, R. A. C.; Nájera, C.; Costa, P. R. R.; *Synthesis* **2015**, *47*, 3505.
16. de Paiva, Y. G.; Silva, T. L.; Xavier, A. F. A.; Cardoso, M. F. C.; da Silva, F. C.; Silva, M. F. S.; Pinheiro, D. P.; Pessoa, C.; Ferreira, V. F.; Goulart, M. O. F.; *J. Braz. Chem. Soc.* **2019**, *30*, 658.
17. Becke, A. D.; *J. Chem. Phys.* **1993**, *98*, 5648.
18. Schaefer, A.; Huber, C.; Ahlrichs, R.; *J. Chem. Phys.* **1994**, *100*, 5829.
19. Chai, J.-D.; Head-Gordon, M.; *Phys. Chem. Chem. Phys.* **2008**, *10*, 6615.
20. Chai, J.-D.; Head-Gordon, M.; *J. Chem. Phys.* **2008**, *128*, 84106.
21. Tomasi, J.; Mennucci, B.; Cammi, R.; *Chem. Rev.* **2005**, *105*, 2999.
22. Frisch, M. J.; Trucks, G. W.; Schlegel, H. B.; Scuseria, G. R.; Robb, M. A.; Cheeseman, J. R.; Scalmani, G.; Barone, V.; Mennucci, B.; Petersson, G. A.; Nakatsuji, H.; Caricato, M.; Li, X.; Hratchian, H. P.; Izmaylov, A. F.; Blonio, J.; Zheg, G.; Sonnenberg, J. L.; Hada, M.; Ehara, M.; Toyota, K.; Fukuda, R.; Hasegawa, J.; Ishida, M.; Nakajima, T.; Honda, Y.; Kitao, O.; Nakai, H.; Vreven, T.; Montgomery, J. A.; Peralta, J. E.; Ogliaro, F.; Bearpark, M.; Heyd, J. J.; Brothers, E.; Kundin, K. N.; Staroverov, V. N.; Keith, T.; Kobayashi, R.; Normand, J.; Raghavachari, K.; Rendell, A.; Burant, J. C.; Iyengar, S. S.; Tomasi, J.; Cossi, M.; Rega, N.; Millam, J. M.; Klene, M.; Knox, J. E.; Cross, J. B.; Bakken, V.; Adamo, C.; Jaramillo, J.; Gomperts, R.; Stratmann, R. E.; Yazyev, O.; Austin, A. J.; Cammi, R.; Pomelli, C.; Ochterski, J. W.; Martin, R. L.; Morokuma, K.; Zakrzewski, V. G.; Voth, G. A.; Salvador, P.; Dannenberg, J. J.; Dapprich, S.; Daniels, A. D.; Farkas, O.; Foresman, J. B.; Ortiz, J. V.; Cioslowski, J.; Fox, D. J.; *Gaussian09, Revision D.01*; Gaussian, Inc., Wallingford, CT, 2013.
23. Song, Y.; Buettner, G. R.; *Free Radical Biol. Med.* **2010**, *49*, 919; Augusto, O.; Miyamoto, S. In *Principles of Free Radical Biomedicine*, vol. 1; Pantopoulos, K.; Schipper, H. M., eds.; Nova Science Publishers, Inc.: Hauppauge, NY, 2011, p. 19; Antunes, F.; Salvador, A.; Marinho, H. S.; Alves, R.; Pinto, R. E.; *Free Radical Biol. Med.* **1996**, *21*, 917; Nohl, H.; Jordan, W.; *Bioorg. Chem.* **1987**, *15*, 374.
24. Moore, H. W.; Czerniak, R.; *Med. Res. Rev.* **1981**, *1*, 249.
25. Barker, B.; Diao, L.; Wan, P. J.; *J. Photochem. Photobiol., A* **1997**, *104*, 91.
26. Skibo, E. B. In *Quinone Methides*, vol. 1; Rokita, S. E., ed.; Wiley: Hoboken, 2009, p. 217; Toteva, M.; Richard, J. P.; *Adv. Phys. Org. Chem.* **2011**, *45*, 39; Wellington, W.; *RSC Adv.* **2015**, *5*, 20309; Amouri, H.; *Synlett* **2011**, *10*, 1357.
27. Cao, S.; Peng, X.; *Curr. Org. Chem.* **2014**, *18*, 70.
28. Liška, A.; Rosenkranz, M.; Klíma, J.; Dunsch, L.; Lhoták, P.; Ludvík, J.; *Electrochim. Acta* **2014**, *140*, 572; Squella, J. A.; Bollo, S.; Nunez-Vergara, L. J.; *Curr. Org. Chem.* **2005**, *9*, 565.
29. Laurent, A. D.; Jacquemin, D.; *Int. J. Quantum Chem.* **2013**, *11*, 2019.

Submitted: March 19, 2019

Published online: July 16, 2019

